Pérez, JJ.; Ewertowska, E.; Berjano, E. (2020). Computer modeling for radiofrequency bipolar ablation inside ducts and vessels: Relation between pullback speed and impedance progress. Lasers in Surgery and Medicine. 52(9):897-906. https://doi.org/10.1002/lsm.23230

Computer modeling for radiofrequency bipolar ablation inside ducts and vessels: Relation between pullback speed and impedance progress

Juan J. Pérez[1], Elżbieta Ewertowska[1], Enrique Berjano[1]*

[1]*BioMIT, Department of Electronic Engineering, Universitat Politècnica de València, Valencia, Spain*

***Corresponding author:** Dr. Enrique Berjano, Department of Electronic Engineering (Building 7F), Universitat Politècnica de València, Camino de Vera, 46022 Valencia, Spain. Email: eberjano@eln.upv.es

Contract grant sponsor: *Spanish Ministerio de Ciencia, Innovación y Universidades* under "*Programa Estatal de I+D+i Orientada a los Retos de la Sociedad.*" **Contract grant number:** RTI2018-094357-B-C21. **Contract grant sponsor:** Predoctoral Grant from Ministry of Economy, Industry and Competitiveness (Government of Spain). **Contract grant number:** BES-2015–073285. **Contract grant sponsor:** United States Air Force Office of Scientific Research.

Conflicts of Interest Disclosures: All authors have completed and submitted the ICMJE Form for Disclosure of Potential Conflicts of Interest and none were reported.

Short running: Modeling for RF bipolar ablation inside ducts and vessels

ABSTRACT

Objectives: Radiofrequency (RF)-induced ablation can be carried out inside ducts and vessels by simultaneously dragging a bipolar catheter while applying RF power. Our objective was to characterize the relation between pullback speed, impedance progress and temperature distribution.

Methods: We built a numerical model including a bipolar catheter which is dragged inside a duct while RF power is applied between a pair of electrodes. The model solved a triple coupled electrical, thermal and mechanical problem. Lesions were assessed by an Arrhenius model. The numerical model's thermal and electrical characteristics were chosen to obtain the same initial impedance value as in the experiments: 560 Ω at 16ºC (sample temperature).

Results: When pullback speed was too slow (<0.4 mm/s) impedance continued to drop when the catheter began to move, creating deep lesions, overheating and impedance roll-off, while at the faster speed (0.4 to 1.0 mm/s) impedance first rose slightly and then reached a plateau. There was a strong inverse relation between pullback speed and lesion depth. The hottest point was always around the second electrode, creating a kind of hot wake.

Conclusions: These findings confirm the close relationship between pullback speed and impedance progress, and suggest that the latter factor could be used to guide the procedure and achieve effective and safe ablations along the inner path of a duct or vessel.

Key words: Ablation, computer model, duct, numerical model, radiofrequency ablation.

1. Introduction

Radiofrequency (RF)-induced ablation is performed inside vessels and ducts as a minimally-invasive RF technique to treat a variety of different diseases. In some cases, such as the treatment of varicose veins [1], the objective of endovascular RF ablation is to create a thermal lesion around the lumen and along a segment of the vein to achieve its closure. Intraductal RF ablation has been proposed to manage primary and secondary bile duct tumors [2] and treat malignant obstructions in the biliary and pancreatic ducts [3], since it has a thermal effect that re-channels the malignant obstruction through coagulation while the immunomodulatory effect controls tumor re-growth, thus potentially delaying tumor development [4]. Note that in these cases the ablation electrodes occupy more or less the entire duct lumen, and therefore should not be confused with the case in which the ablation is performed on the wall of a duct whose diameter is much larger than that of the electrode. In this second case, the ablation electrodes are usually positioned on an expandable device (e.g. inflated balloon) as in RF ablation (RFA) of Barrett's esophagus [5] and RFA of pulmonary veins to treat atrial fibrillation [6].

In this context, we recently proposed a similar endoductal RF ablation method to seal the pancreatic duct in the context of surgical management of the pancreatic stump after a pancreatectomy as an alternative to other mechanical methods (e.g. sutures, staplers, clips or endoluminal glue injection) [7], the reason being that these methods continue to offer suboptimal results and have relatively high complication rates, especially the development of postoperative pancreatic fistula (POPF) [8]. From a technical point of view, our novel bipolar ablation method involves simultaneously dragging a catheter and transmitting RF power between two electrodes. The impedance progress measured between these two electrodes has been suggested as a control parameter to guide the procedure and is known

to be related to pullback speed. Even though there are studies that claim high success rates in closing varicose veins [9] or sealing the pancreatic duct [7], there is also a recognized need for a better understanding of the relationship between applied power, pullback speed and the created thermal lesion [10]. The long-term goal is to optimize these procedures by implementing automatic pullback-speed control guided by impedance progress. The aim of the present study was to build a numerical model to be used as a test bench for this line of research, i.e. able to predict the thermal lesion and impedance progress at different pullback speeds. The computer results were compared to those obtained from an experimental study on an ex vivo model based on liver fragments. This tissue type has already been used in previous studies on RF-induced ablation of varicose veins since it facilitates the observation of the effect of different withdrawal speeds and power settings on lesion size and shape [10]. In fact, the liver tissue findings were found to be reproducible in a vein using the same settings [11].

2. Materials and methods

2.1. Modeling of the catheter

The study focused on a 5 Fr catheter with four 2mm-long electrodes separated by 5 mm (diagnostic catheter Josephson curve 5-5-5 6 Fr × 2 mm manufactured by Bard Medical (Covington, GA, USA). The distal electrode exactly coincided with the catheter tip (semi-spherical in shape), while electrodes #2, #3 and #4 were ring electrodes. First, a teardown process was conducted to identify the different catheter components and dimensions, since we suspected that much of the heat generated inside the tissue is really evacuated through the electrodes themselves and other inner metal parts such as electric wires and guide-

wires. Detailed information on the inner parts of the catheter therefore seemed to be crucial in building a realistic model. From this we found that the ring electrodes were comprised of 0.18 mm-thick cylindrical metal plates (see Fig. 1A) and more than likely made of platinum-iridium. The following properties were assumed: density (ρ) 21,500 kg/m^3, specific heat (c) 132 J/kg·K, thermal conductivity (k) 71 W/m·K, and electrical conductivity (σ) 4.6×10^6 S/m [12-14]. We also found that the ring electrodes were placed on the surface of a hollow plastic tube ~0.35 mm thick (see Fig. 1A). Although we did not know the exact type of plastic or its properties, many previous cardiac ablation modeling studies assumed it to be polyurethane [12-14] with a density of 70 kg/m^3, specific heat of 1045 J/kg·K and thermal conductivity of 0.026 W/m·K. If we attribute these properties to the entire catheter we are actually ignoring some internal components which could have a thermal impact since they can evacuate heat from the electrodes towards the rest of the catheter. As our idea was to finally model the catheter as a solid cylinder with metal electrodes on its surface, the teardown process provided valuable information on the ρ, c and k values that could reproduce the overall thermal performance of a fragment of catheter and could be applied to the cylinder instead of the values of the polyurethane.

The following analysis was conducted on a catheter fragment without electrodes (see Fig. 1A): first, density was estimated directly by weighing a 100 mm fragment with a given estimated volume, obtaining a value of ρ = 1440 kg/m^3, which is far removed from the value of polyurethane (70 kg/m^3). This could be expected since the catheter really includes denser parts, such as metal wires. However, it must be remembered that the habitual polyurethane values used are really those of polyurethane foam and not those of the solid polyurethane on the outside of the catheter.

After dismantling the catheter fragment we found four electric wires (0.18 mm diameter) inside the plastic tube, probably made of copper, and three twisted alloy wires 0.125 mm in diameter. Although we could not identify the exact type of plastic in the tube, we confirmed that it sank in a saturated dilution of NaCl, which indicated a density slightly above 1200 kg/m^3 and assumed a value of 1300 kg/m^3. This method was chosen since it was extremely difficult to accurately measure the volume of the plastic piece. We assumed a specific heat of 1500 J/kg·K, since most plastics present a value between 1100 and 1800 J/kg·K [15]). The thermal conductivity value habitually employed for polyurethane in modeling studies (0.026 W/m·K) is extremely low, and is actually that of polyurethane foam. For this reason, we assumed a value of 0.3 W/m·K, which is in the range reported for solid polyurethane, (0.1 and 0.5 W/m·K [16]). With these values for the plastic tube and assuming that the three twisted wires were also copper, we estimated an overall value *c* from the percentage weight of each plastic and copper element, obtaining a value of c = 1050 J/kg·K, which is close to that of plastic (1045 J/kg·K) but far from that of copper (380 J/kg·K), since the percentage weight of the metal parts was much lower than the plastic part.

Two 40 cm long models were built to estimate an overall *k* value of the catheter (see Fig. 1B). The same thermal problem was solved in both: a temperature step of 80ºC was applied at the edge of the catheter (initial temperature 25ºC) and temperature progress was analyzed at different points (i.e. $T(x,t)$). The first model ('numerical model', see Fig. 1B) aimed to realistically represent the catheter's thermal performance and was based on two concentric cylinders, one plastic (1.667 mm outer diameter, 0.35 mm thick) and another metal (0.4835 mm outer diameter, 0.048 mm thick). The thickness of the metal cylinder was chosen to represent the same volume as the seven wires described above, so that the central gap was filled with air (0.4355 mm outer diameter). The metal cylinder was assumed to be copper

(ρ = 8820 kg/m^3, c = 380 J/kg·K, k = 360 W/m·K), while the plastic cylinder was assumed to have the properties described above. This model was solved numerically on ANSYS Multiphysics (ANSYS, Canonsburg, PA, USA). The second model ('analytical model', see Fig. 1B) was based on a solid 1.667 mm diameter cylinder (equivalent to 5 Fr) whose density and specific heat were 1440 kg/m^3 and 1050 J/kg·K, respectively (the previously estimated overall parameters), while its thermal conductivity k fluctuated within a certain range. This was because we used the 'analytical model' based on homogenous material to estimate a global value of k for the entire catheter. Due to its homogeneity, the thermal solution was analytically obtained and is described in the Annex. The results of the 'numerical model' were compared with those of the 'analytical model' at different thermal conductivity values, temperature progress at points from x = 5 cm to x = 25 cm. The best fit was obtained when the thermal conductivity of the 'analytical model' was 23 W/m·K, which is surprisingly higher than the value of most plastics (from 0.1 to 0.5 W/m·K). However, this could be expected since the catheter conducts heat in its longitudinal direction, probably due to the influence of the metal wires (k values above 100 W/m·K).

In the following sections the catheter is modeled as a solid material with the following overall properties: ρ = 1440 kg/m^3, c = 1050 J/kg·K and k = 23 W/m·K. Note that these are not really plastic values, but those of a material able to mimic the thermal performance of a catheter segment containing four electric wires. Obviously, the values could be expected to vary slightly for the segment between electrodes #4 and #3 (with one less wire) and between #3 and #2 (with two less wires), etc.

2.2. Model with biological tissue

Figure 2A shows the physical situation in which the catheter is completely inserted into the tissue and passes through a hole with a diameter identical to that of the catheter. Note the axial symmetry around the longitudinal catheter axis. Fig. 2B shows the geometry of the model which included a 5 Fr catheter that slipped inside a duct with the same diameter as the catheter (1.667 mm). The catheter had four electrodes (2 mm long) separated by 5 mm. The first electrode was modeled as the solid metal distal point of the catheter, while the remaining electrodes were modeled as 0.18 mm thick cylindrical bands. The axial symmetry simplifies the problem to a 2D model. A convergence test showed that the outer tissue dimensions (W and H in Fig. 2B) were large enough to keep the tissue surfaces at boundary tissue temperature and voltage. The value of the maximum temperature (T_{max}) reached in the tissue after 20 s was used as a control parameter for this test. Consecutive simulations were conducted by increasing both parameters (W and H) in 1 mm steps. When the difference in the T_{max} between consecutive simulations was less than 0.5% we considered the dimensions W and H obtained in the preceding step to be adequate. Catheter pullback was modeled over a total length of 77 mm, since this was the exact length of the catheter used in the experiments.

2.2. Governing equations and boundary conditions

The model, based on a coupled electric-thermal-mechanical problem, was solved numerically by the Finite Element Method (FEM) with ANSYS software (ANSYS, Canonsburg, PA, USA). The governing equation for the thermal problem was the classical heat transfer equation:

$$\rho c \frac{\partial T}{\partial t} = \nabla \cdot (k \nabla T) + q_{RF} \qquad (1)$$

where ρ is density (kg/m^3), c specific heat (J/kg·K), T temperature (ºC), t time (s), k thermal conductivity (W/m·K), and q_{RF} the heat source caused by RF power (W/m^3). Since we are modeling an ex vivo experiment the blood perfusion and metabolic heat terms are obviously absent. Tissue vaporization was modeled by modifying Eq. (1) for temperatures between 99 and 100ºC, as described in [17,18] and including a value of 2.17·109 J/m^3·K for water's latent heat of vaporization multiplied by water density at 100ºC, which coincides with that of liver tissue [19].

The biological medium can be considered almost totally resistive at RF frequencies (~500 kHz) and over the distance of interest since the displacement currents are much less important than the conduction currents, which enables a quasi-static approach to solving the electrical problem. The distributed heat source q_{RF} is given by $q = \sigma|\boldsymbol{E}|^2$, where $|\boldsymbol{E}|$ is the magnitude of the vector electric field (V/m) and σ the electrical conductivity (S/m). $\boldsymbol{E} = -\nabla\Phi$ is calculated from the gradient of the voltage Φ(V), which, in absence of internal electric sources, satisfies $\nabla\cdot(\sigma\nabla\Phi) = 0$. The thermal lesion dimensions were estimated by the Arrhenius damage model, which associates temperature with exposure time by a first-order kinetics relationship:

$$\Omega(t) = \int_0^t A e^{-\frac{\Delta E}{RT}} ds \qquad (2)$$

where R is the universal gas constant, A (7.39×10^{39} s^{-1}) is a frequency factor and ΔE (2.577×10^5 J/mol) is the activation energy for the irreversible damage reaction. We employed the Ω = 1 contour to assess the geometry and dimensions of the thermally damaged tissue zone. We had previously shown that this combination of parameters is a good representation of the whitish zone of the ex vivo liver [20].

Boundary conditions are represented in Fig. 2C. Thermal boundary conditions were: null thermal flux in the transversal direction to the symmetry axis ($\frac{\partial T}{\partial r}=0$) and constant temperature T_s = 16ºC in the tissue boundaries (temperature of the ex vivo samples). Electrical boundary conditions were: Zero current density in the transverse direction to the symmetry axis and tissue boundaries ($I=\frac{\partial V}{\partial r}=0$). RF power was applied between the third and fourth electrodes, for which we set zero voltage in one electrode and 43 V in the other (as in the ex vivo experiments).

The model mesh was heterogeneous with a finer mesh size at the electrode-tissue interfaces, where the highest electrical and thermal gradients were expected. All the mesh elements used were triangular in the tissue and rectangular in the catheter. Suitable mesh size and time-step were assessed by means of a convergence test with the same characteristics as those used for the outer geometry dimensions. The model had 30,022 nodes and 14,180 elements (triangular in the tissue and rectangular in the electrodes).

2.3. Tissue characteristics

The results of a preliminary ex vivo study [21] were used to adjust the values of the tissue electrical characteristics in the computer model (electrical conductivity and its temperature dependence). Samples of porcine liver were acquired from a local slaughterhouse. This type of tissue was chosen for its accessibility, homogeneity and ease of identifying the shape of thermal lesions. Ablations were conducted using a 5 Fr catheter (1.667 mm diameter) placed between two slices of tissues. A voltage of 43 V was applied between two metal electrodes (2 mm long separated by 5 mm) using a Radionics Cosman Coagulator CC-1

(Radionics, Burlington, MA, USA). Impedance evolution was recorded during the ablations by a USB data acquisition module connected to the RF generator. The pullback started once the impedance reached a plateau (value more or less stable). The initial impedance value recorded in the ex vivo study was used to adjust tissue electrical conductivity (σ) in the computer model, while the impedance progress during the phase in which catheter was at rest was used to adjust the temperature dependence of σ. The metal electrodes were considered to have a $\sigma = 4.6 \cdot 10^6$ S/m, while the catheter shaft was considered to be a plastic material with $\sigma = 10^{-5}$ S/m.

The thermal characteristics of the tissue were those of liver [22]: thermal conductivity (k) 0.52 W/m·K, density (ρ) 1079 kg/m^3 and specific heat (c) 3540 J/kg·K. The mechanical properties of tissue and catheter were unrealistically chosen to have tissue and catheter completely non-deformable, i.e. the catheter was assumed to slip along the tissue surface without producing deformation.

Tissue electrical conductivity was assumed to change with temperature as described in Zurbuchen et al [23], who experimentally found different behavior of porcine liver electrical conductivity in the heating and cooling phases. In the former, it first increases linearly at a rate of +1.6 %/°C from the initial temperature to 75°C, then changes gradually from 75°C to 85°C, reaching a maximum value at 80°C, and finally drops at a rate of –1.6 %/°C from 85°C to 99°C. In the cooling phase, electrical conductivity decreases at a rate of –0.84 %/°C.

2.4. Modeling catheter movement

First of all, it is important to point out that we did not really solve a mechanical problem involving changes in geometry or mesh. Since we were only interested in solving the electrical-thermal coupled problem while the catheter was moving, we indirectly assumed two perfect solids (catheter and tissue). For the mesh of both solids we used the PLANE223 coupled-field element (ANSYS) specifically selecting the 'structural-thermoelectric' coupling. Since we were not interested in modeling the mechanical interaction between catheter and tissue, we assigned the same mechanical properties to both solids with the sole objective of making the catheter slide through the hole. We considered the mechanical properties of the platinum and iridium alloy (Young's modulus 172.37 GPa and Poisson's ratio 0.38) in particular in order to avoid any mechanical deformation caused by dragging the catheter. Likewise, we used the TARGE169 and CONTA172 elements (ANSYS) to manage the behavior of the contact surfaces in electrical and thermal terms. We chose values high enough for thermal contact conductance and electrical contact conductance in order to achieve almost negligible differences of temperature and voltages between both solids (< 0.5%).

2.5. Analyzed cases

The tissue electrical characteristics from previous ex vivo experiments (as described in Section 2.3) were used to conduct computer simulations, modeling catheter pullback at different speeds from 0.1 mm/s to 1.0 mm/s. Computation times varied from 16 hours for 1.0 mm/s, to 44 hours for 0.4 mm/s (values lower than 0.4 mm/s caused roll-offs and premature cessation of power application).

3. Results

3.1. Estimation of electrical characteristics

The initial impedance reported in [21] was 568±48 Ω. Once RF application started, impedance was gradually reduced to a more or less stable value of 334±37 Ω in ~20 s. Considering the initial temperature of the samples (16ºC) we obtained a value σ = 0.28 S/m (assessed at 20ºC) which allowed an initial impedance of exactly 568 Ω. A change of σ at a temperature of +1.6%/ºC reproduced the impedance progress obtained in the experiments (see Fig. 3A).

Besides the thermal properties of the catheter, Fig. 3A also shows the impedance progress in a simulation in which the catheter properties were assumed to be those of polyurethane foam. When the catheter had low thermal inertia (due to very low density and thermal conductivity, 70 kg/m^3 and 0.026 W/m·K, respectively), impedance dropped faster, which was associated with faster heating, as confirmed by the temperature plots in Fig. 3B. The catheter properties chosen to build the model obtained a clearly better agreement between the computer and experimental results.

3.2. Impedance progress during pullback

Figure 4 shows the impedance progress for different pullback speeds ranging from 0.1 mm/s to 1.0 mm/s. All the cases began with a period of 20 seconds in which the catheter was at rest, so that all the cases from this period coincide. From then on, two different behaviors were observed: at low speeds (0.1 to 0.3 mm/s) impedance continued to fall to a minimum of ~225 Ω and then rose at an increasing rate to exceed the initial value, causing a roll-off about 20 s after the initial movement. This stopped the power application at 41, 43 and 49 s at pullback speeds of 0.1, 0.2 and 0.3 mm/s, respectively, and made it impossible

to complete a long thermal lesion.

At higher speeds (0.4 mm/s to 1.0 mm/s) impedance fell slightly (almost negligible at higher speeds), and increased until reaching a value where it remained for the rest of the process. The value of this plateau was higher at high speeds (e.g. ~340 Ω for 0.4 mm/s vs. ~400 Ω for 1.0 mm/s) and the lesions could be completed.

3.3. Temperature distribution during pullback

Figure 5 shows the temperature distributions around the RF electrodes during the early pullback stage (0.7 mm/s). It can be seen that when the second electrode reaches the spot previously occupied by the first, this zone receives 'extra heating', which increases lesion depth and the total lesion thus shows a thickening in the start zone (see lesion boundaries on Fig. 6). Regardless of pullback speed, temperature distribution along the path always shows an extra heating effect around the second electrode, a phenomenon we might call 'hot wake'. Later, at speeds high enough to avoid roll-offs (0.4 mm/s onwards), with both electrodes at a distance from the start zone, lesion depth stays more or less constant along the path (see Fig. 6).

Figure 7 shows the lesion depth around the electrode at different speeds. As pullback speed increases, lesion depth decreases. For instance, at 0.4 mm/s the lesion was 1.8 mm deep and at 1.0 mm/s it was just 0.4 mm. We found a strong linear relationship between pullback speed and lesion depth (R2=99%). With roll-offs due to extremely low speed (0.3 mm/s and less) lesions were shorter but relatively deep (~2 mm), regardless of speed.

4. Discussion

An endoductal bipolar RF ablation computer model was built and simulations were carried out to characterize the relation between pullback speed, impedance progress and temperature distribution. Although our motive was to develop a catheter-based technique to seal the pancreatic duct, we reasonably inferred that this model could be equally useful to study the technique's electrical and thermal performance in other ducts and veins. In fact, to our knowledge, this is the first numerical model able to reproduce the electrical and thermal behavior of RF bipolar ablation by a catheter operating inside a duct or vessel. The proposed model can quantify the relationship between pullback speed, applied power and temperature distributions around the duct or vessel. Although a previous model had already been developed for RF ablation of varicose veins [24], it fell short of our objectives for several reasons: 1) it did not consider the geometry shown in Fig. 1, in which the catheter completely occupies the duct lumen, but instead a thin catheter in the center of the vessel with blood flowing around the electrode; and 2) it did not solve the electrical problem, but assumed the electrode surfaces to be the source of heat for keeping the temperature constant at 85ºC, and so was not able to compute impedance progress during RF heating.

In the present study, the electrical conductivity of the tissue was set to match the initial impedance between experiments and simulations. The value found (0.28 S/m) was within the range reported in the database (0.221±0.352 S/m) [22]. Once we had obtained a model able to mimic impedance progress reasonably well with the catheter at rest (see Fig. 3), we conducted computer simulations to study the relation between impedance and temperature distributions. The value of the simulated voltage (43 V) was selected because this was used in the preliminary ex vivo study whose results were used to validate the computer model [21] and was obtained after a trial and error process in which we tried to obtain a sufficiently deep thermal lesion (1–2 mm) and avoid overheating and tissue sticking. It thus

seemed reasonable to expect that a lower voltage would create shallower thermal lesions, while a higher value would cause overheating and impedance roll-off.

The computer results showed that when pullback speed is below 0.4 mm/s, impedance continues to fall even when the catheter moves (Fig. 4), which suggests that the tissue continues to heat up. This causes deep lesions (Fig. 6 and 7) and a final roll-off due to the tissue around the electrode becoming completely dehydrated. This agrees with our experimental findings, where we observed that abrupt impedance rises were associated with tissue-sticking and carbonization points [21]. In practical terms they suggest that this overheating could be detected by monitoring the gradual drop in impedance during catheter pullback and that overheating could be avoided at higher pullback speeds.

However, when pullback speed is fast enough (0.4 to 1.0 mm/s), impedance first rises slightly (in direct proportion to speed) until it reaches a constant value (plateau) (see Fig. 4) and therefore does not cause a subsequent roll-off, while lesion depth remains constant. This suggests that pullback speed should be such that impedance remains more or less constant, i.e. in a plateau zone in order to achieve safe and continuous lesions (i.e. without gaps, overheating and subsequent sticking). This was in fact the approach followed in our previous experimental study [21], in which we had to vary speed manually during pullback when we observed that the impedance value deviated from the plateau.

The computer results also suggest that, at least in homogeneous tissue, there is a strong relationship between pullback speed and the lesion depth assessed when impedance reaches a constant value (Fig. 7), when lesion depth remains more or less constant. As expected, the lower the speed the deeper the lesion because RF power is applied for longer in the same zone. It is interesting to note the relatively broad range of possible lesion depths to be programmed, from very shallow (less than 0.5 mm) to 2 mm. These results are also in

agreement with the findings of the experimental study concerning an approximate mean pullback speed (0.7 mm/s) and lesion depth (1 mm) [21]. Although we did not study the effect of applied voltage, it is logical to assume that its effect is also important. In this respect, due to we simulated constant-voltage ablations, applied power depended on the tissue impedance, which also depended on pullback speed. For instance, once impedance reached the plateau, power applied ranged from 5.4 W in case of 0.4 mm/s (340 Ω), to 4.6 W in the case of 1.0 mm/s (400 Ω). We then can compute the 'linear endovenous energy density' parameter (LEED), which is determined by multiplying power applied (in W) by the pullback speed (in s/cm), giving the amount of energy transmitted into 1 cm of treated duct/vein (in J/cm) [11]. Our LEED values ranged from 46 J/cm in the case of 1.0 mm/s (4.6 W × 10 s/cm), to 135 J/cm in the case of 0.4 mm/s (5.4 W × 25 s/cm). These values are in general much higher than those normally used for RF vein ablation, which typically range from 18 to 25 J/cm, derived from an applied power of 18–25 W and pullback speed of 10 mm/s [11]. Overall, our setting for sealing the pancreatic duct is based on much less power (~5 W instead of ~20 W) and a much slower pullback (0.4–1 mm/s instead of 10 mm/s). This was possibly due to the slow speed, allowing the operator (or the possible future automatic system) to rapidly detect any impedance changes during ablation and to modify speed accordingly to avoid overheating and tissue sticking. If the speed is low, the power has to be low enough to prevent overheating.

However, since the LEED value already takes both power and speed into account, the explanation for the differences between our values and those used in vein treatment lies in the different electrode arrangements. If we focus on the treatment of varicose veins and consider, for instance, the CelonProCurve 1200-S15 catheter (Celon AG medical

instruments, Teltow, Germany), although it has a similar diameter (1.8 mm) to ours (1.667 mm) the arrangement is very different, a 4-mm distal electrode 2 mm from a 9-mm proximal electrode (offering a total 'active length' of 15 mm), while ours considered two identical 2-mm electrodes separated by 5 mm, with a total 'active length' of 9 mm. The effective electrode surfaces in both arrangements are clearly different: 20.9 mm^2 in our case and 73.5 mm^2 in the case of CelonProCurve catheter.

This difference has a huge effect on current density around the electrode, with more or less localized heating: the smaller electrode/tissue contact surface gives higher current density values, so that the power in our application was lower than that for varicose veins. It should be remembered that the phenomenon is clearly non-linear with energy, and that the lesion characteristics in fact depend on the specific set of parameters chosen (power and time). For instance, unlike our case, a comparable LEED value (100 J/cm) implemented in the CelonProCurve catheter produced continuous roll-offs [10] and the CelonProCurve's lower power produced very shallow lesions [25], while ours were adequate.

Our simulations provided information on the temperature distributions around the electrodes. As shown in Fig. 5, when the second electrode reaches a position previously covered by the first, the zone has already been heated, has higher electrical conductivity and hence is more prone to dissipate RF power. This means that the hottest point is precisely around the second electrode, creating a kind of hot wake. This suggests that if a temperature sensor were to be embedded in the catheter, the best position would be in the second electrode.

Limitations of the study

One of the study's main limitations was the question of tissue homogeneity, which meant

that lesion depth was uniform along the entire ablation trajectory. It is reasonable to assume that thermal lesions would be somewhat irregular in tissue with different electrical and thermal properties. Future computer studies should be carried out to mimic thermal performance in the presence of tissue zones of different characteristics. In fact, in these circumstances the computer model would provide information on modulating pullback speed to achieve regular lesions, for example, and to compensate for impedance variations in order to keep it in the plateau. It is also important to point out that the modeling study ignored the mathematical terms associated with metabolic heat and blood perfusion. In this respect, it is well known that including the blood perfusion term implies an additional mechanism to evacuate heat (blood perfusion rate of pancreas is not negligible, 767±357 mL/min/kg [22]), and hence the lesion dimensions would be smaller than those computed without blood perfusion, while the metabolic heat term implies an additional heat source. However, its value (11.89 W/kg for pancreas [22]) is in fact negligible compared to the power applied by the RF catheter (~5 W restricted to an extremely small volume around the electrodes).

Our model assumed that the electrodes are in direct contact with the tissue, which is exactly what is expected in the case of endoluminal RF ablation of the pancreatic duct, since the idea is that the catheter diameter should be slightly smaller than that of the lumen. In this way there is practically no gap between electrode and tissue and we make sure that the electric current passes through the tissue to create an effective thermal lesion. However, if this were not the case, we would have a gap filled with pancreatic juice between electrodes and tissue so that the RF current would circulate mainly through juice instead of tissue, impeding the creation of an effective thermal lesion.

Although our model was limited to a segment of 77 mm, the conclusions should remain valid for any length. In theory, RF pancreatic duct ablation should be conducted on the longest possible segment. It is reasonable to assume that the longer the segment the smaller the pancreatic juice spillage and the lower the risk of pancreatic leakage. However, there may be an inherent technical limitation, as the main duct narrows close to the tail of the pancreas.

Finally, it should be recognized that many of the estimated parameters in the model present wide variations. Despite this, the model was not developed to predict lesion depth under specific conditions, but to qualitatively study the relationship between pullback speed, impedance progress and temperature distributions, so that it is reasonable to assume that the dispersion of the parameter values will not produce results that seriously invalidate the conclusions.

5. Conclusions

The computer results confirm the close relationship between pullback speed and impedance progress during pullback of an RF catheter inside a duct or vessel. When pullback speed was too slow (<0.4 mm/s) impedance continued to drop when the catheter began to move, creating deep lesions, overheating and impedance roll-off, while at the faster speed (0.4 to 1.0 mm/s) impedance first rose slightly and then reached a plateau. Qualitatively, it is interesting to note that the hottest point is always around the second electrode, creating a kind of hot wake. The model can be used in future studies to explore how impedance progress could be used to guide the procedure and achieve effective and safe ablations along the inner path of a duct or vessel.

References

1. Boon R, Akkersdijk GJ, Nio D. Percutaneus treatment of varicose veins with bipolar radiofrequency ablation. Eur J Radiol. 2010;75(1):43–7.
2. Atar M, Kadayifci A, Daglilar E, Hagen C, Fernandez-Del Castillo C, Brugge WR. Ex vivo human bile duct radiofrequency ablation with a bipolar catheter. Surg Endosc. 2018 Jun;32(6):2808-2813.
3. Larghi A, Rimbaş M, Tringali A, Boškoski I, Rizzatti G, Costamagna G. Endoscopic radiofrequency biliary ablation treatment: A comprehensive review. Dig Endosc. 2019 May;31(3):245-255.
4. Mizandari M, Kumar J, Pai M, Chikovani T, Azrumelashvili T, Reccia I, Habib N. Interventional radiofrequency ablation: A promising therapeutic modality in the management of malignant biliary and pancreatic duct obstruction. J Cancer. 2018 Jan 5;9(4):629-637.
5. Belghazi K, Pouw RE, Koch AD, Weusten BLAM, Schoon EJ, Curvers WL, Gotink AW, Mostafavi N, Haidry RJ, Pech O, Bergman JJGHM, Bisschops R. Self-sizing radiofrequency ablation balloon for eradication of Barrett's esophagus: results of an international multicenter randomized trial comparing 3 different treatment regimens. Gastrointest Endosc. 2019 Sep;90(3):415-423.
6. Gianni C, Chen Q, Della Rocca D, Canpolat U, Ayhan H, MacDonald B, Mohanty S, Trivedi C, Natale A, Al-Ahmad A. Radiofrequency Balloon Devices for Atrial Fibrillation Ablation. Card Electrophysiol Clin. 2019 Sep;11(3):487-493.
7. Andaluz A, Ewertowska E, Moll X, Aguilar A, García F, Fondevila D, Quesada R, Berjano E, Grande L, Burdío F. Endoluminal radiofrequency ablation of the main pancreatic duct is a secure and effective method to produce pancreatic atrophy and to achieve stump closure. Sci Rep. 2019;9(1):5928.
8. Burdío F, Dorcaratto D, Hernandez L, Andaluz A, Moll X, Quesada R, Poves I, Grande L, Cáceres M, Berjano E. Radiofrequency-induced heating versus mechanical stapler for pancreatic stump closure: in vivo comparative study. Int J Hyperthermia. 2016 May;32(3):272-80.
9. Braithwaite B, Hnatek L, Zierau U, Camci M, Akkersdijk G, Nio D, Sarlija M, Ajduk M, Santoro P, Roche E. Radiofrequency-induced thermal therapy: results of a European multicentre study of resistive ablation of incompetent truncal varicose veins. Phlebology. 2013;28(1):38–46.
10. Badham GE, Strong SM and Whiteley MS. An in vitro study to optimise treatment of varicose veins with radiofrequency-induced thermotherapy. Phlebology 2015;30:17–23.

11. Badham GE, Dos Santos SJ, Whiteley MS. Radiofrequency-induced thermotherapy (RFiTT) in a porcine liver model and ex vivo great saphenous vein. Minim Invasive Ther Allied Technol. 2017 Aug;26(4):200-206.
12. Panescu D, Whayne JG, Fleischman SD, Mirotznik MS, Swanson DK, Webster JG. Three-dimensional finite element analysis of current density and temperature distributions during radio-frequency ablation. IEEE Trans Biomed Eng. 1995;42(9):879–90.
13. Jain MK, Wolf PD. A three-dimensional finite element model of radiofrequency ablation with blood flow and its experimental validation. Ann Biomed Eng. 2000;28(9):1075–84.
14. Tungjitkusolmun S, Woo EJ, Cao H, Tsai JZ, Vorperian VR, Webster JG. Thermal--electrical finite element modelling for radio frequency cardiac ablation: effects of changes in myocardial properties. Med Biol Eng Comput. 2000;38(5):562–8.
15. https://www.engineeringtoolbox.com/specific-heat-capacity-d_391.html (accessed in July 26th, 2019)
16. https://www.engineeringtoolbox.com/thermal-conductivity-d_429.html (accessed in July 26th, 2019)
17. Abraham JP, Sparrow EM. A thermal-ablation bioheat model including liquid-to-vapor phase change, pressure- and necrosis-dependent perfusion, and moisture-dependent properties. Int J Heat Mass Transfer 2007;50:2537–44.
18. Trujillo M, Berjano E. Review of the mathematical functions used to model the temperature dependence of electrical and thermal conductivities of biological tissue in radiofrequency ablation. Int J Hyperthermia. 2013 Sep;29(6):590-7.
19. Trujillo M, Bon J, José Rivera M, Burdío F, Berjano E. Computer modelling of an impedance-controlled pulsing protocol for RF tumour ablation with a cooled electrode. Int J Hyperthermia. 2016 Dec;32(8):931-939.
20. Pérez JJ, Pérez-Cajaraville JJ, Muñoz V, Berjano E. Computer modeling of electrical and thermal performance during bipolar pulsed radiofrequency for pain relief. Med Phys. 2014 Jul;41(7):071708.
21. Ewertowska E, Andaluz A, Moll X, Aguilar A, Garcia F, Fondevila D, Quesada R, Trujillo M, Burdío F, Berjano E. Development of a catheter-based technique for endoluminal radiofrequency sealing of pancreatic duct. Int. J Hyperthermia. 2019;36(1):677–86.
22. Hasgall PA, Di Gennaro F, Baumgartner C et al. 2016. IT'IS Database for thermal and electromagnetic

parameters of biological tissues, Version 3.0, September 1st, 2015, www.itis.ethz.ch/database (accessed May 3rd, 2019).

23. Zurbuchen U, Holmer C, Lehmann KS, Stein T, Roggan A, Seifarth C, Buhr HJ, Ritz JP. Determination of the temperature-dependent electric conductivity of liver tissue ex vivo and in vivo: Importance for therapy planning for the radiofrequency ablation of liver tumours. Int J Hyperthermia. 2010;26(1):26–33.

24. Choi SY, Kwak BK, Seo T. Mathematical modeling of radiofrequency ablation for varicose veins. Comput Math Methods Med. 2014;2014:485353.

25. Reich-Schupke S, Mumme A, Stücker M. Histopathological findings in varicose veins following bipolar radiofrequency-induced thermotherapy--results of an ex vivo experiment. Phlebology. 2011 Mar;26(2):69-74.

Annex

The analytical model considered a solid cylinder with a negligible diameter value compared to its length. This length is large enough so that temperature changes at one end do not cause temperature changes at the other. In such conditions, we can model the catheter as a semi-infinite line so that the heat conduction responds to the equation

$$\frac{\partial T}{\partial t} = a^2 \frac{\partial^2 T}{\partial x^2} \tag{1}$$

$T(x,t)$ being the temperature at a time t and at a point x of the line; and a being:

$$a = \sqrt{\frac{k}{C \cdot \rho}} \tag{2}$$

where k is thermal conductivity, C the specific heat, and ρ the density.

The boundary conditions employed to solve Eq. (1) were: initial temperature $T(x,0) = T_0$, temperature step of value T_S at x=0 (i.e. $T(0,t) = T_S$, for $t > 0$).

From [1A], the solution for Eq (1) is:

$$T(x,t) = T_S \cdot (1 - G(u)) + T_0 \cdot G(u) \tag{3}$$

G being the Gauss error function:

$$G(u) = \frac{2}{\pi} \cdot \int_0^u e^{-\alpha^2} d\alpha \tag{4}$$

and

$$u = \frac{x}{2 \cdot \sqrt{a^2 t}} \tag{5}$$

[1A] Tijonov AN, Samarsky AA. Equations of Mathematical Physics. Dover Publications Inc., 2011.

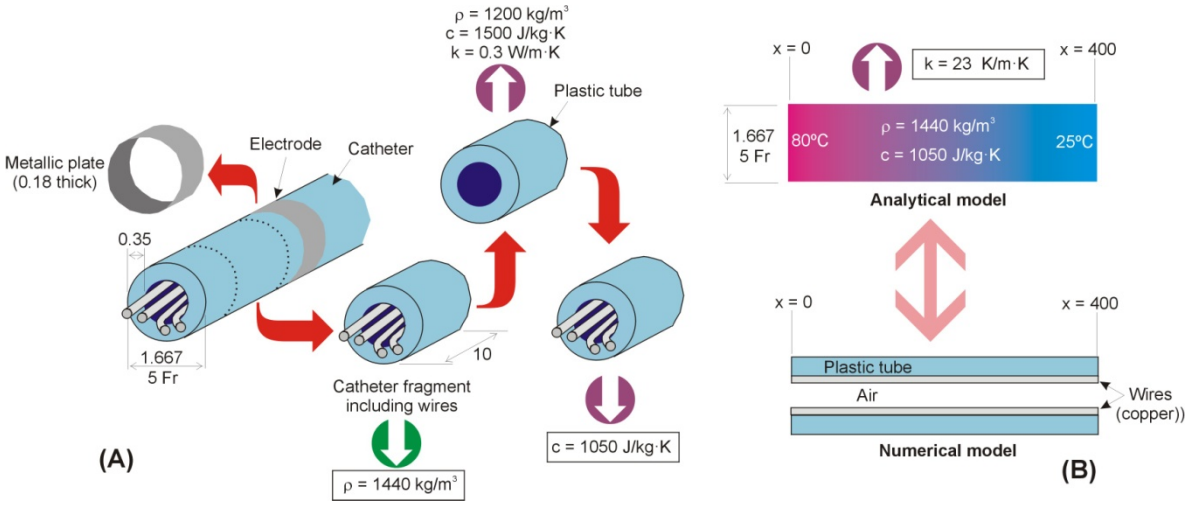

Figure 1 **A:** Chart showing the roadmap followed in the teardown process and how a set of overall parameters were estimated for a full segment of catheter including internal wires (boxed values). **B:** Analytical and numerical models used to estimate the overall value of thermal conductivity (see text for more details).

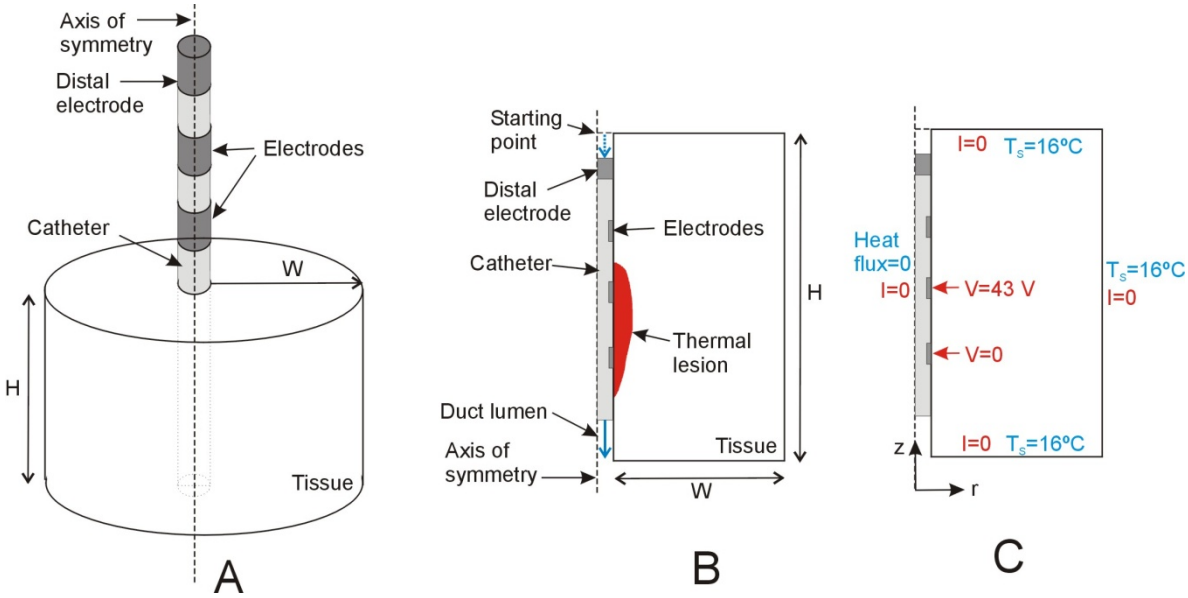

Figure 2 **A:** Physical situation considered in the study. **B:** Model geometry comprised of a catheter dragged inside a duct (W=40 mm, H=100 mm). Blue arrows show the direction of movement. RF power is applied between electrodes #3 and #4. **C:** Electrical (red) and thermal (blue) boundary conditions used in the computer model.

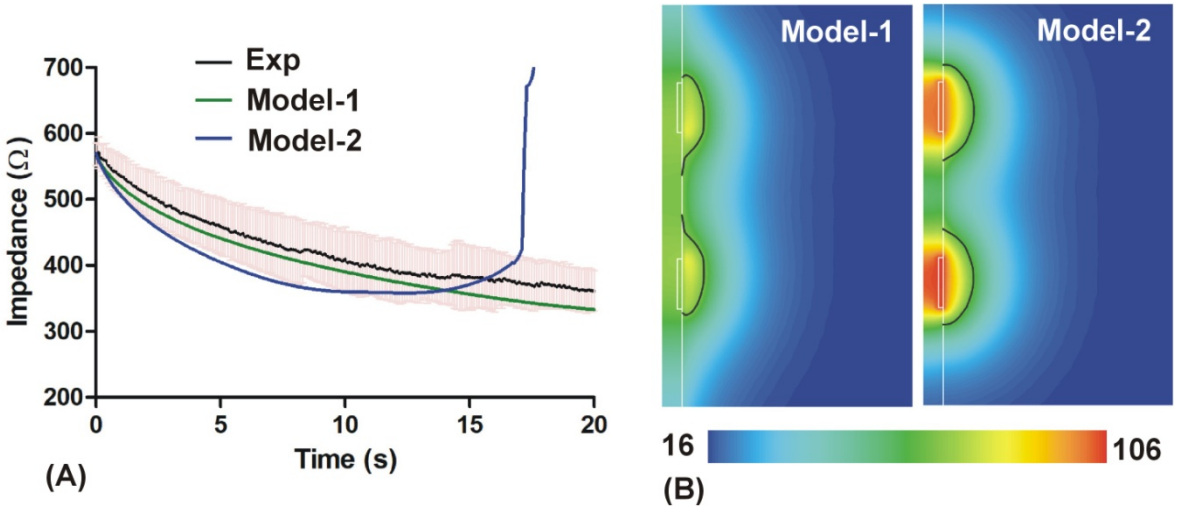

Figure 3 **A:** Impedance progress during the first 20 seconds of bipolar ablation without catheter pullback. Black line represents the mean values of the experiments (n=15), while green and blue lines show the computer results. In Model-2 the catheter body was assumed to have the characteristics of polyurethane [5-7], while in Model-1 the characteristics were estimated from measurements and assumptions (see text for details). **B:** Temperature distributions for both models at 18 s (when maximum temperature reaches 100ºC in Model-2). Black line represents the thermal lesion boundary (Ω=1).

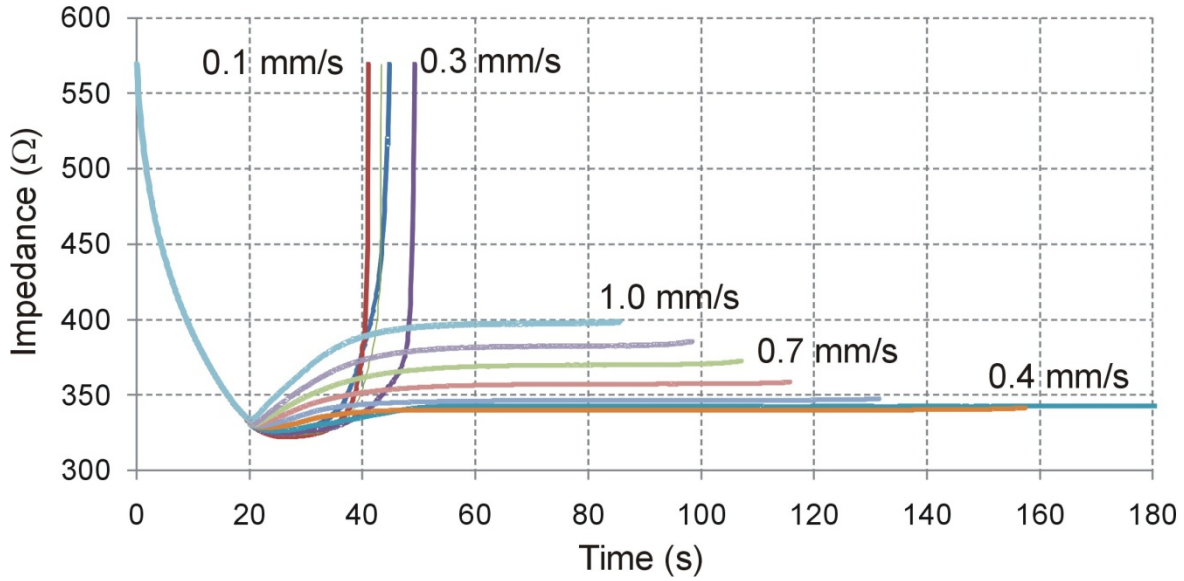

Figure 4 Impedance progress during bipolar ablation at different pullback velocities. The first 20 seconds are common to all the cases since the catheter remains at rest. Note roll-off occurred around 40 s at low velocities (0.1 to 0.3 mm/s). In the other cases, note that as speed increased ablation was reduced because the segment was ablated sooner (e.g. 85 s for 1.0 mm/s vs. 180 s for 0.4 mm/s).

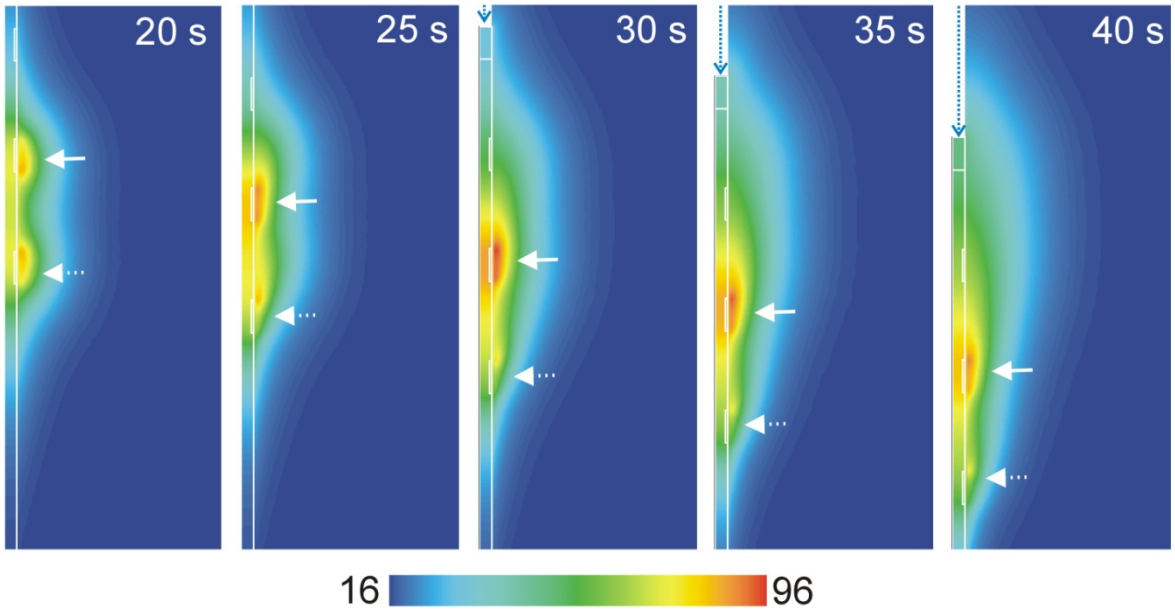

Figure 5 Evolution of the temperature distributions around the electrodes for a pullback speed of 0.7 mm/s. Solid and dashed arrows indicate the position of the second and first electrode, respectively. Blue arrows indicate catheter movement through the inside of the duct. When the second electrode reaches the position previously covered by the first, extra heating occurs in this area and there is a hot wake during the pullback. In other words, the thermal lesion is mainly caused by the second electrode.

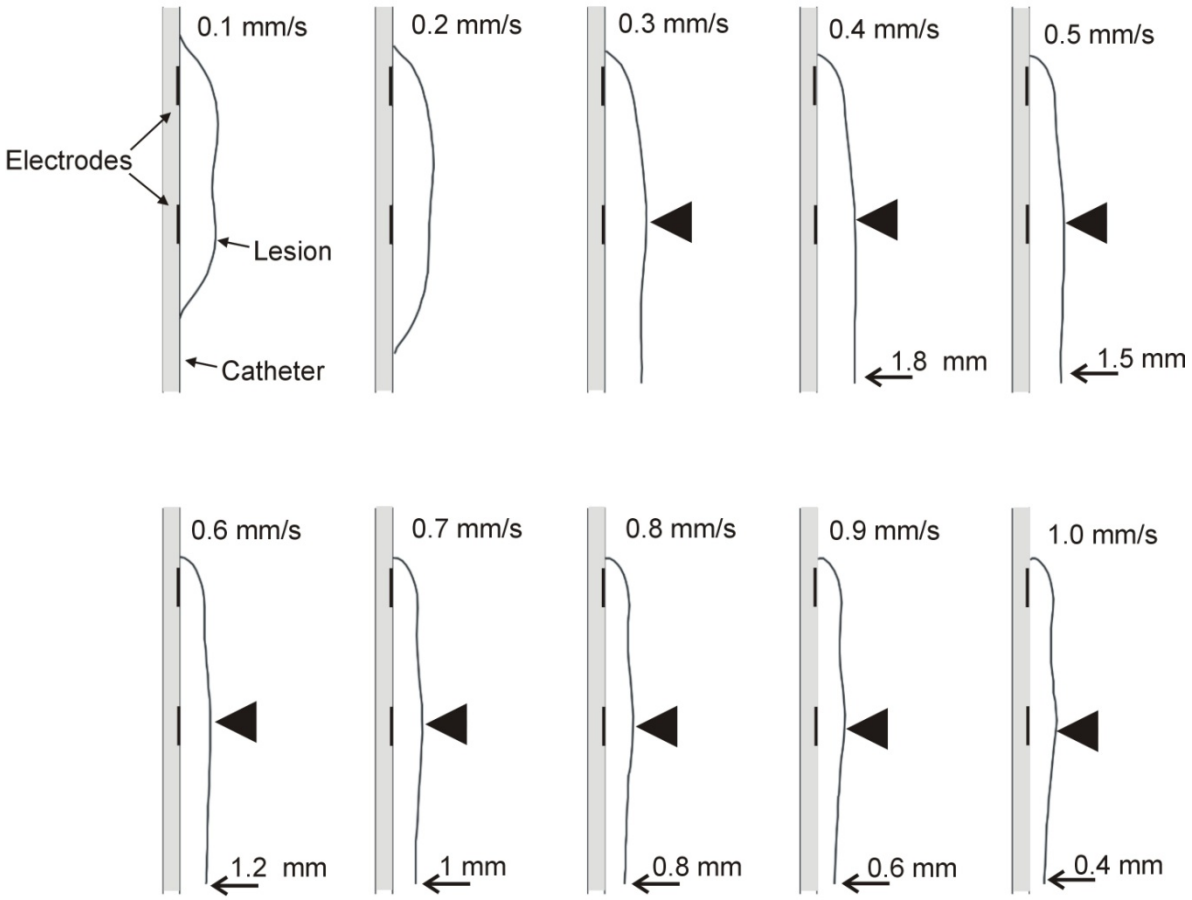

Figure 6 Lesion boundaries for different pullback speeds (black solid line) at the end of the ablation. In the cases of 0.1, 0.2 and 0.3 mm/s, ablations ceased prematurely at 41, 43 and 49 s, respectively, so that lesion boundaries were computed for these times. Grey rectangle represents the catheter and thin black rectangles represent electrode positions and start of pullback. The bottom arrows indicate lesion depth in the area where it becomes more or less constant. Note that the lesion is always deeper in a zone initially occupied by the first electrode (arrowheads).

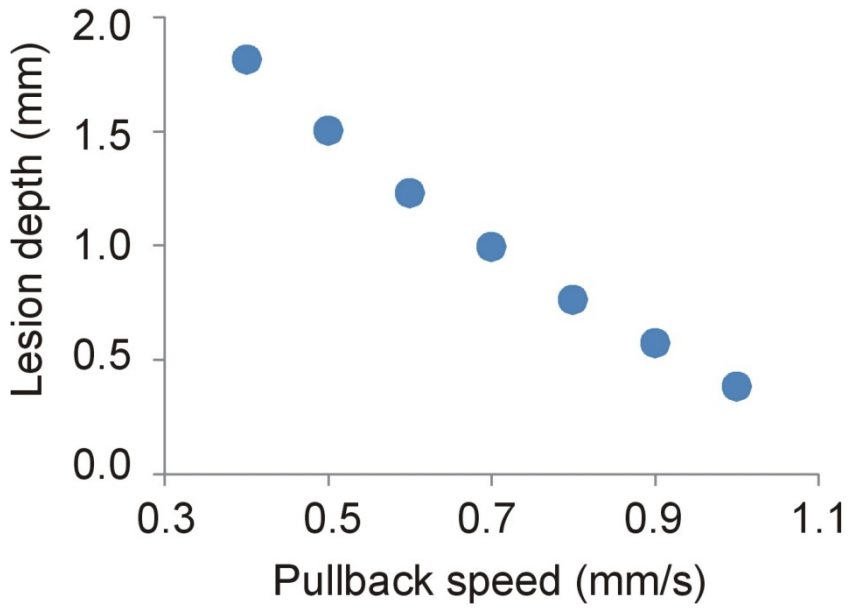

Figure 7 Relation between thermal lesion depth LD (measured from the electrode surface in the segment where it is constant) and pullback speed (PS). The curve of best fit followed the linear equation: LD = –2.37·PS + 2.70 (R2=0.99).